INTERNATIONAL JOURNAL FOR NUMERICAL METHODS IN FLUIDS
Int. J. Numer. Meth. Fluids 2000; **33**: 23–34

A new numerical study of the shock/boundary-layer interaction

Yiqing Shen[a,1], Ruquan Wang[b,*] and Hongzhi Liao[a]

[a] *Department of Mathematics, Yunnan University, Kunming 650091, China*
[b] *Institute of Computational Mathematics and Scientific/Engineering Computing, Academia Sinica, Beijing 100080, China*

SUMMARY

This paper describes a new numerical study of the flat plate shock/boundary-layer interaction by using a weighted high-resolution, total variation diminishing (TVD) scheme. The key difference of this study from former studies is that new secondary vortices in the separated region have been found for the first time, with increasing the impinging shock angle or the free-stream Mach number. Copyright © 2000 John Wiley & Sons, Ltd.

KEY WORDS: shock/boundary-layer interactions; TVD scheme; WENO scheme

1. INTRODUCTION

The flat plate shock/boundary-layer interaction problem has become a benchmark of testing new numerical methods for viscous flow since the work of MacCormack in 1971 [1]. MacCormack, and others that followed, made many numerical simulations of the flat plate shock/boundary-layer interactions for a fixed set of the free-stream parameters of $M_\infty = 2.0$, $Re_\infty = 2.96 \times 10^5$ and an impinging shock angle of 32.585°. In this case, the flow will induce a separated region with a primary vortex upon the flat plate. Up to 1989, Liou [2] investigated the effect of the shock strength and the Reynolds number on the separation and found that the transverse velocity component behind the incident shock is also an important parameter. Liou did a series of computations for different impinging shock angles of $\beta = 31.376°$, 32.008°, 32.663°, 33.342° and 34.047°, and then gave the corresponding figures of the effect of the shock angles on surface pressure and friction coefficient at the fixed $M_\infty = 2.0$ and $Re_\infty = 2.96 \times 10^5$. Unfortunately, Liou did not find the appearance of a secondary vortex for $\beta = 34.047°$. The present new numerical study has shown that the secondary vortices will be induced in the

* Correspondence to: Institute of Computational Mathematics and Scientific/Engineering Computing, Academia Sinica, PO Box 2719, Beijing 100080, China.
[1] Current address: Institute of Mechanics, Academia Sinica, Beijing 100080, China.

Received 3 August 1997
Revised 12 February 1999

primary vortex, when $\beta \geq 34.047°$ for $M_\infty = 2.0$ and $Re_\infty = 2.96 \times 10^5$ or $M_\infty > 2.0$ for the specified $Re_\infty = 2.96 \times 10^5$ and $\beta = 32.585°$. This paper will also analyse the effect of the shock angle, Mach number and grids on the secondary vortices, and give the corresponding flow patterns.

2. FORMULATION OF PROBLEM

Consider the two-dimensional shock/boundary-layer interactions on the flat plate, as in Figure 1.

When an oblique shock wave with sufficient strength impinges on a laminar boundary layer, the boundary layer will induce a separated region and result in a complex viscous flow field.

The inflow boundary is the free-stream conditions, all flow variables at the outflow boundary are extrapolated with second-order accuracy. At the top boundary, the free-stream conditions are used ahead of the impinging shock wave and all variables are specified by the shock relations behind the shock wave. Along the flat plate, $u = 0$, $v = 0$, $\partial p/\partial n = 0$, $\partial T/\partial n = 0$ are employed. Other computational parameters are $\gamma = 1.4$, $Pr = 0.72$.

Following Reference [4], a computational domain is chosen to be $0 \leq x \leq 0.32$ and $0 \leq y \leq 0.1215$. The flat plate is introduced from $x = 0.03$.

3. THE GOVERNING EQUATIONS

The time-dependent two-dimensional Navier–Stokes equations in Cartesian co-ordinates are written as follows:

$$\frac{\partial U}{\partial t} + \frac{\partial F}{\partial x} + \frac{\partial G}{\partial y} = \frac{\partial F_v}{\partial x} + \frac{\partial G_v}{\partial y} \tag{3.1}$$

where U is a vector of the conserved variables, F and G are the inviscid fluxes, F_v and G_v are the viscous fluxes

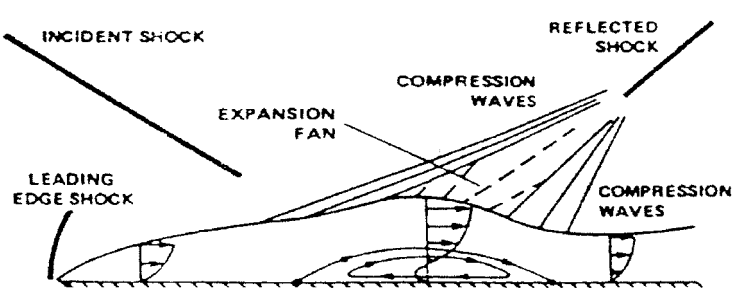

Figure 1. Sketch of shock/boundary-layer interaction.

$$U = (\rho, \rho u, \rho v, \rho e_t)^T$$

$$F = (\rho u, \rho u^2 + p, \rho uv, (\rho e_t + p)u)^T$$

$$G = (\rho v, \rho uv, \rho v^2 + p, (\rho e_t + p)v)^T$$

$$F_v = (0, \tau_{xx}, \tau_{xy}, u\tau_{xx} + v\tau_{xy} + q_x)^T$$

$$G_v = (0, \tau_{xy}, \tau_{yy}, u\tau_{xy} + v\tau_{yy} + q_y)^T$$

$$e_t = e + \frac{1}{2}(u^2 + v^2)$$

The components of the shear stress tensor have the form

$$\tau_{xx} = \frac{\mu}{Re_\infty} \cdot \frac{2}{3}(2u_x - v_y)$$

$$\tau_{xy} = \frac{\mu}{Re_\infty} \cdot (u_y + v_x)$$

$$\tau_{yy} = \frac{\mu}{Re_\infty} \cdot \frac{2}{3}(2u_y - u_x)$$

and the components of the heat flux vector are

$$q_x = \frac{\mu}{Re_\infty(\gamma - 1)M_\infty^2 Pr} \cdot T_x, \qquad q_y = \frac{\mu}{Re_\infty(\gamma - 1)M_\infty^2 Pr} \cdot T_y$$

where Pr is the Prandtl number, M_∞ is the Mach number and Re_∞ is the Reynolds number.

Equation (3.1) has been non-dimensionalized in the following way:

$$x = \frac{\bar{x}}{\bar{L}}, \quad y = \frac{\bar{y}}{\bar{L}}, \quad t = \frac{\bar{t}}{\bar{L}/\bar{u}_\infty}, \quad u = \frac{\bar{u}}{\bar{u}_\infty}, \quad v = \frac{\bar{v}}{\bar{v}_\infty}, \quad e = \frac{\bar{e}}{\bar{u}_\infty^2}, \quad \rho = \frac{\bar{\rho}}{\bar{\rho}_\infty}, \quad p = \frac{\bar{p}}{\bar{\rho}_\infty \cdot \bar{u}_\infty^2},$$

$$T = \frac{\bar{T}}{\bar{T}_\infty}, \quad \mu = \frac{\bar{\mu}}{\bar{\mu}_\infty}$$

where $\bar{L} = 0.16$ is a reference length.

The equation of state is

$$T = \frac{\gamma M_\infty^2 p}{\rho} \tag{3.2}$$

and the Sutherland formula for the coefficient of viscosity, μ, is employed in the present computation

$$\mu = T^{3/2}\frac{1-c}{T+c} \tag{3.3}$$

where $c = 110.4k/\bar{T}_\infty$.

Using the generalized co-ordinates transformation

$$\xi = \xi(x, y), \qquad \eta = \eta(x, y)$$

the Navier–Stokes equations (3.1) may be rewritten as follows:

$$\frac{\partial \tilde{U}}{\partial t} + \frac{\partial \tilde{F}}{\partial \xi} + \frac{\partial \tilde{G}}{\partial \eta} = \delta\left(\frac{\partial \tilde{F}_v}{\partial \xi} + \frac{\partial \tilde{G}_v}{\partial \eta}\right) \tag{3.4}$$

where $\delta = 0$ and 1 represent the parabolized Navier–Stokes (PNS) and fully Navier–Stokes (NS) equations respectively.

$$\bar{U} = \frac{U}{J}$$

$$\tilde{F} = \frac{(\xi_x F + \xi_y G)}{J}, \qquad \tilde{G} = \frac{(\eta_x F + \eta_y G)}{J}$$

$$\tilde{F}_v = \frac{(\xi_x F_v + \xi_x G_v)}{J}, \qquad \tilde{G}_v = \frac{(\eta_x F_v + \eta_y G_v)}{J}$$

$$J = \frac{\partial(\xi, \eta)}{\partial(x, y)} = \xi_x \eta_y - \xi_y \eta_x$$

In this paper a simple co-ordinate transformation is used

$$\begin{cases} \xi = x \\ \eta = 1 - \dfrac{\ln\left(\dfrac{\beta_1 + 1 - y_1}{\beta_1 - 1 + y_1}\right)}{\ln\left(\dfrac{\beta_1 + 1}{\beta_1 - 1}\right)} \end{cases} \tag{3.5}$$

where $\beta_1 = 1.002$ is a parameter of grid density, $y_1 = y/h$ and $h = 0.1215$ is the height of the computational domain.

4. NUMERICAL METHODS

In this paper an explicit–implicit algorithm is employed for solving Equation (3.4), i.e. the difference scheme is explicit in the ξ-direction and implicit in the η-direction, in which the boundary layer near the wall will play an important role. In order to capture accurately shock waves in the flow field, a weighted form of the Roe-type scheme is applied for the inviscid part of Equation (3.4) and central difference is applied for the viscous part. As a result, the resulting system of difference equations can be solved by using the sub-routine for a block tridiagonal system of equations. The semi-discrete conservative difference scheme has the following form:

$$\left(\frac{\partial \tilde{U}}{\partial t}\right)_{ij}^{n+1} + \frac{\tilde{F}_{i+1/2,j}^{n} - \tilde{F}_{i-1/2,j}^{n}}{\Delta\xi} + \frac{\tilde{G}_{i,j+1/2}^{n+1} - \tilde{G}_{i,j-1/2}^{n+1}}{\Delta\eta} = \delta \frac{\tilde{F}_{v_{i+1/2,j}}^{n} - \tilde{F}_{v_{i-1/2,j}}^{n}}{\Delta\xi} + \frac{\tilde{G}_{v_{i,j+1/2}}^{n+1} - \tilde{G}_{v_{i,j-1/2}}^{n+1}}{\Delta\eta} \tag{4.1}$$

Based on the idea of the WENO difference scheme [3], the weighted Roe-type scheme is described for a set of one-dimensional conservative hyperbolic equations

$$\left(\frac{\partial \tilde{U}}{\partial t}\right)_{j}^{n+1} + \frac{H_{j+1/2} - H_{j-1/2}}{\Delta\xi} = 0 \tag{4.2}$$

where

$$\begin{aligned} H_{j+1/2} = {} & \frac{1}{2}(\tilde{F}_{j+1} + \tilde{F}_{j} - R_{j+1/2}|\Lambda_{j+1/2}|R^{-1}_{j+1/2}\Delta\tilde{U}_{j+1/2}) \\ & + \frac{1}{2} R_{j+1/2}(\Omega_1^{+}\Lambda^{+}_{j+1/2}R^{-1}_{j+1/2}\Delta\tilde{U}_{j+1/2} + \Omega_2^{+}\Lambda^{+}_{j-1/2}R^{-1}_{j-1/2}\Delta\tilde{U}_{j-1/2}) \\ & - \frac{1}{2} R_{j+1/2}(\Omega_1^{-}\Lambda^{-}_{j+1/2}R^{-1}_{j+1/2}\Delta\tilde{U}_{j+1/2} + \Omega_2^{-}\Lambda^{-}_{j+3/2}R^{-1}_{j+3/2}\Delta\tilde{U}_{j+3/2}) \end{aligned} \tag{4.3}$$

where $A = \partial\tilde{F}(\tilde{U})/\partial\tilde{U}$, $A = R\Lambda R^{-1}$ and R is a right eigenvector matrix of A. $\Omega_1^{\pm}$, $\Omega_1^{\pm}$ and $\Lambda^{\pm}_{j+1/2}$ are diagonal matrices, and

$$\begin{aligned} & \Omega_k^{\pm} = \mathrm{diag}(\omega_k^{1\pm}, \omega_k^{2\pm}, \omega_k^{3\pm}, \omega_k^{4\pm}), \quad k = 1, 2 \\ & \Lambda^{\pm}_{j+1/2} = \mathrm{diag}\left(\frac{\lambda^1_{j+1/2} \pm |\lambda^1_{j+1/2}|}{2}, \frac{\lambda^2_{j+1/2} \pm |\lambda^2_{j+1/2}|}{2}, \frac{\lambda^3_{j+1/2} \pm |\lambda^3_{j+1/2}|}{2}, \frac{\lambda^4_{j+1/2} \pm |\lambda^4_{j+1/2}|}{2}\right) \\ & \omega_1^{i\pm} = \frac{\beta_1^{i\pm}}{\beta_1^{i\pm} + \beta_2^{i\pm}}, \qquad \omega_2^{i\pm} = \frac{\beta_2^{i\pm}}{\beta_1^{i\pm} + \beta_2^{i\pm}} \end{aligned} \tag{4.4}$$

$$\beta_1^{i\pm} = \frac{1}{\varepsilon + \left| \frac{\lambda_{j+1/2}^i + |\lambda_{j+1/2}^i|}{2} \alpha_{j+1/2}^i \right|}, \qquad \beta_2^{i+} = \frac{1}{\varepsilon + \left| \frac{\lambda_{j-1/2}^i + |\lambda_{j-1/2}^i|}{2} \alpha_{j-1/2}^i \right|}$$

$$\beta_1^{i-} = \frac{1}{\varepsilon + \left| \frac{\lambda_{j+1/2}^i - |\lambda_{j+1/2}^i|}{2} \alpha_{j+1/2}^i \right|}, \qquad \beta_2^{i-} = \frac{1}{\varepsilon + \left| \frac{\lambda_{j+3/2}^i - |\lambda_{j+3/2}^i|}{2} \alpha_{j+3/2}^i \right|},$$

$$i = 1, 2, 3, 4 \tag{4.5}$$

where

$$\alpha_{j+1/2} = R_{j+1/2}^{-1} \Delta \tilde{U}_{j+1/2} = (\alpha_{j+1/2}^1, \alpha_{j+1/2}^2, \alpha_{j+1/2}^3, \alpha_{j+1/2}^4)^T$$

$R_{j+1/2}$, $R_{j+1/2}^{-1}$ and $\Lambda_{j+1/2}^{\pm}$ are computed by using Roe's averages.

The variable ε is a positive real number that is introduced to avoid the denominator becoming zero; in this paper, $\varepsilon = 10^{-10}$.

5. NUMERICAL RESULTS AND ANALYSIS

Some numerical results of the flat plate shock/boundary-layer interactions are presented for different free-stream Mach numbers and impinging shock angles at a specified $Re_\infty = 2.96 \times 10^5$.

(a) $M_\infty = 2.0$, $Re_\infty = 2.96 \times 10^5$, $T_\infty = 293$ K and different shock angles of $\beta = 32.585°$, 32.663°, 33.342°, 34.047°, 34.50° and 35.50°;
(b) $M_\infty = 2.1$, $Re_\infty = 2.96 \times 10^5$, $T_\infty = 293$ K and $\beta = 32.585°$;
(c) $M_\infty = 2.2$, $Re_\infty = 2.96 \times 10^5$, $T_\infty = 293$ K and $\beta = 32.585°$.

For case (a), it was found that when $\beta < 34.047°$, the separated region contains only a primary vortex, which has been captured numerically by previous studies (see Figure 2; when $\beta \geq 34.047°$, a new secondary vortex located in the primary vortex has been observed and was enlarged by increasing the shock angle for the specified M_∞ and Re_∞. A variation of the secondary vortices is clearly displayed in Figures 2–5, 9 and 10 for a grid of 65×65. Notice that Liou [2] did not find the appearance of a small secondary vortex for $\beta = 34.047°$, even though a finer grid of 75×65 was used in that computation.

Furthermore, for the specified Reynolds number and shock angle of $Re_\infty = 2.96 \times 10^5$ and $\beta = 32.58°$, the effect of free-stream Mach number on the vortex structure was also studied. As a result, it was found that when $M_\infty > 2.0$, a new secondary vortex occurred in the primary vortex and was enlarged by increasing the Mach number M_∞. Figures 6 and 7 show such a variation of the secondary vortices. The same grid of 65×65 was adopted in this computation.

In order to analyse the effect of the grid on vortex structure, three grids of 33×33, 65×65 and 129×129 were applied to simulate the flat plate shock/boundary-layer interaction problem by using the weighted Roe-type scheme. The coarsest grid, 33×33, did not capture

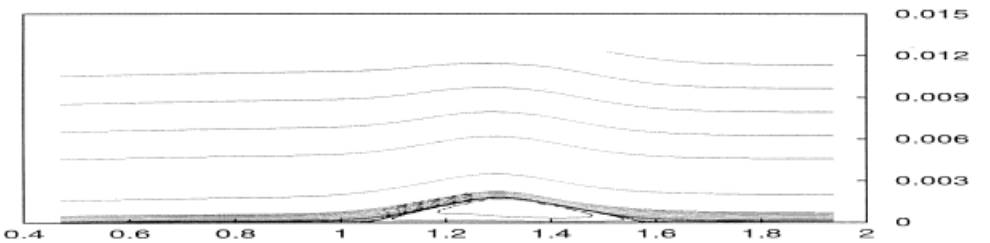

Figure 2. Streamlines ($\beta = 32.585°$ and $M_\infty = 2.0,\ 65 \times 65$).

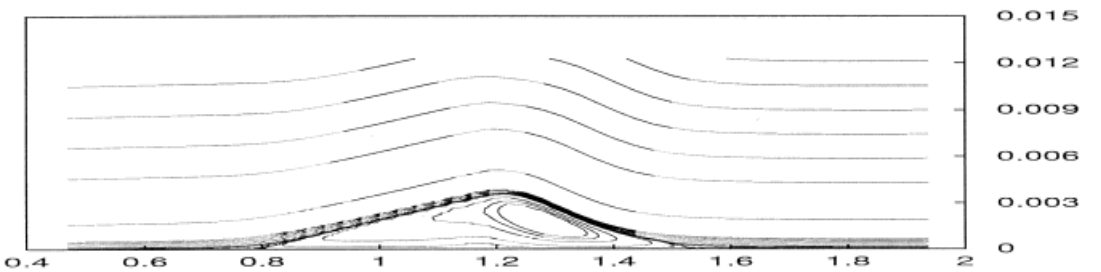

Figure 3. Streamlines ($\beta = 34.047°$ and $M_\infty = 2.0,\ 65 \times 65$).

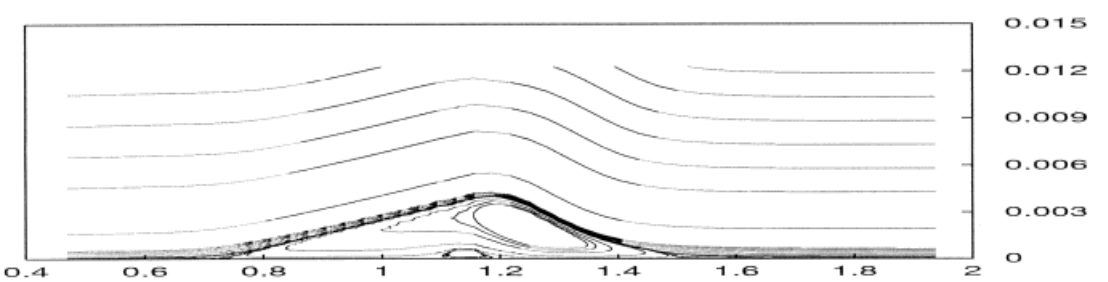

Figure 4. Streamlines ($\beta = 34.5°$ and $M_\infty = 2.0,\ 65 \times 65$).

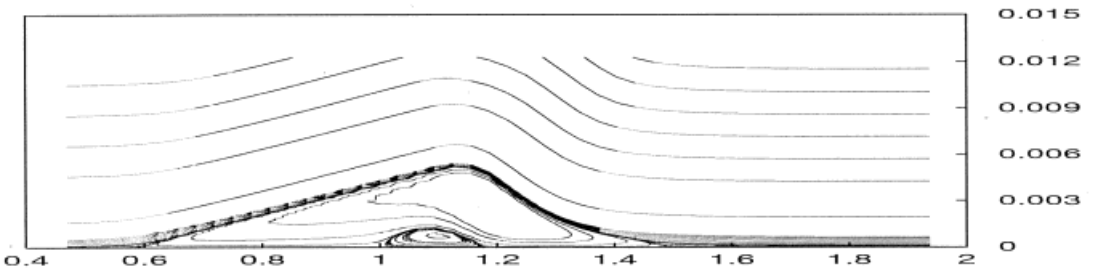

Figure 5. Streamlines ($\beta = 35.5°$ and $M_\infty = 2.0,\ 65 \times 65$).

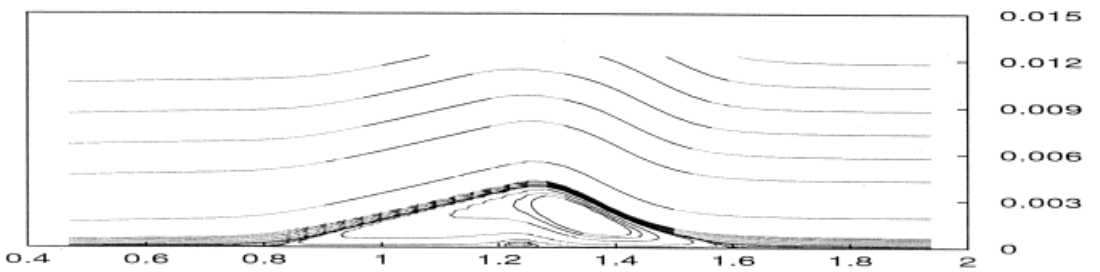

Figure 6. Streamlines ($\beta = 32.585°$ and $M_\infty = 2.1,\ 65 \times 65$).

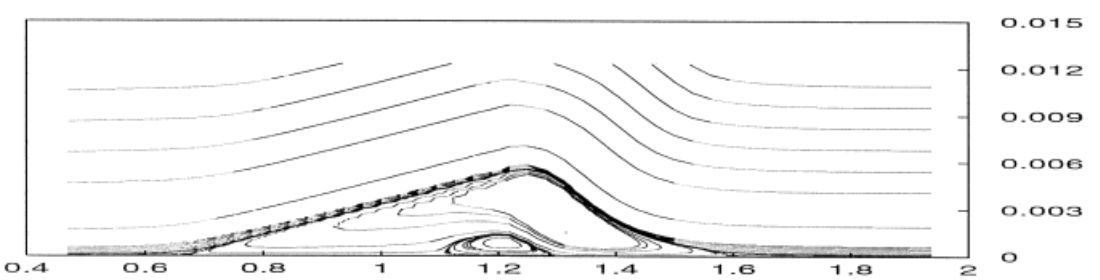

Figure 7. Streamlines ($\beta = 32.585°$ and $M_\infty = 2.2,\ 65 \times 65$).

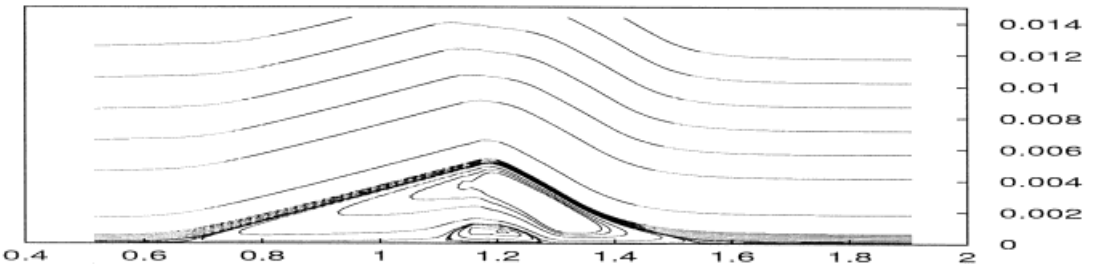

Figure 8. Streamlines ($\beta = 34.5°$ and $M_\infty = 2.0$, 129×129).

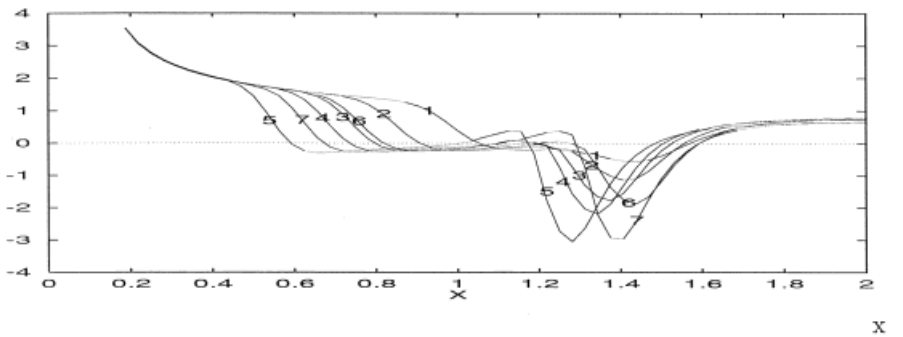

Figure 9. Skin friction distribution on plate, 65×65.

the secondary vortex for $\beta = 34.047°$. Numerical results show that both finer grids of 65×65 and 129×129 have the same vortex structure, but the grid of 129×129 yields a slightly larger primary vortex and a larger secondary vortex. This can be seen from Figures 4, 8, 11 and 12.

Many numerical experiments have shown that the second-order-accurate total variation diminishing (TVD) schemes have the capability of accurately capturing shock discontinuities in inviscid and viscous flow fields, but they cannot simulate correctly separated vortices and complicated viscous flow fields. The reason is due to the first-order accuracy of the TVD schemes at the extremum points. Like the WENO schemes [3], the weighted TVD schemes used in this paper have three desirable features: (1) they improve the accuracy of the original TVD schemes and keep the same non-oscillatory property near the discontinuities; (2) they yield smoother numerical fluxes, which are important for the fast convergence to steady solution; (3) they reduce the heavy usage of logical statements appearing in the TVD schemes. All these features have been validated by the present numerical experiments.

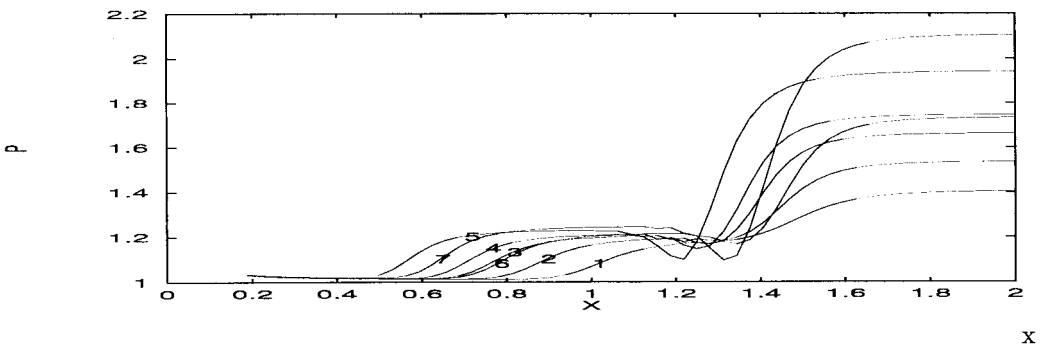

Figure 10. Pressure distribution on plate, 65×65; 1, $\beta = 32.585°$ and $M_\infty = 2.0$; 2, $\beta = 33.342°$ and $M_\infty = 2.0$; 3, $\beta = 34.047°$ and $M_\infty = 2.0$; 4, $\beta = 34.5°$ and $M_\infty = 2.0$; 5, $\beta = 35.5°$ and $M_\infty = 2.0$; 6, $\beta = 32.585°$ and $M_\infty = 2.1$; 7, $\beta = 32.585°$ and $M_\infty = 2.2$.

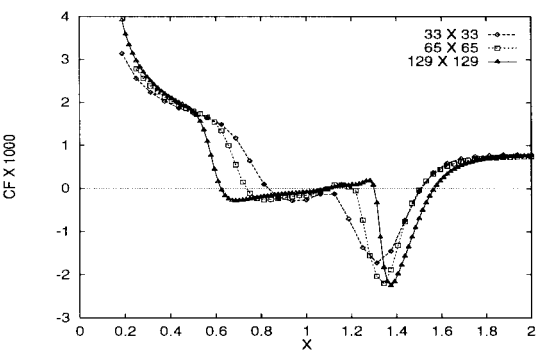

Figure 11. Skin friction distributions on plate. Comparison of three different grids with $\beta = 34.5°$ and $M_\infty = 2.0$.

Notice that the weighted Roe-type scheme, (4.2) and (4.3), enhances the accuracy of the original Roe-type scheme at the extremum points and near the vortices. However, the weighted scheme is a second-order accurate. In order to demonstrate this fact, the flat plate shock/boundary-layer interaction problem has been simulated for the grid 65×65 by using the Roe-type scheme [5], the weighted Roe-type scheme and the third-order Chakravathy–Osher scheme [6]. From Figures 13 and 14, it can be seen that the weighted Roe-type scheme yields numerical solutions located between the Roe-type scheme and Chakravathy–Osher scheme. Among all these schemes, the weighted scheme has a faster convergence rate, so it is more efficient for the computation with a finer grid.

All the computations in this paper were carried out by the NS equations. Comparison of the full NS equations and PNS equations showed that numerical solutions have only small differences if the Reynolds number is large enough. The comparative results will be given in another paper.

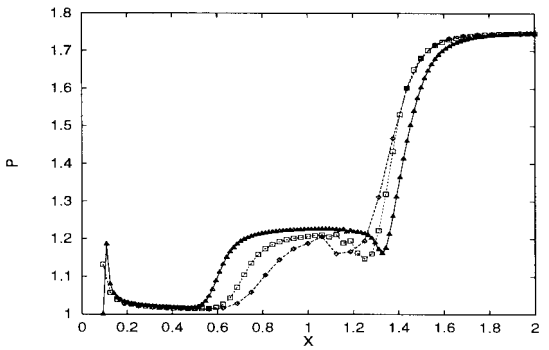

Figure 12. Pressure distributions on plate. Comparison of three different grids with $\beta = 34.5°$ and $M_\infty = 2.0$.

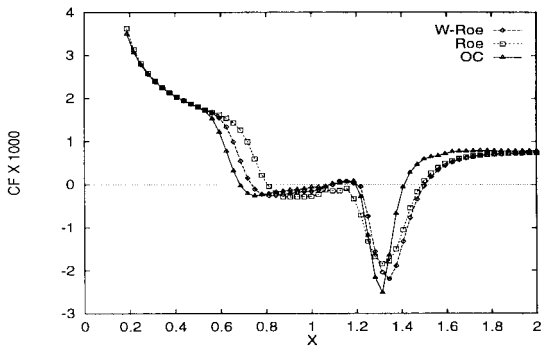

Figure 13. Skin friction distributions on plate. Comparison of three different grids with $\beta = 34.5°$ and $M_\infty = 2.0,\ 65 \times 65$.

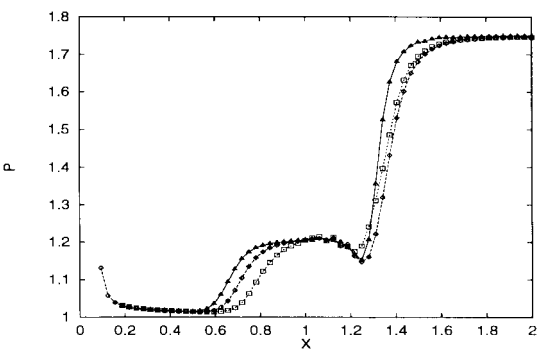

Figure 14. Pressure distributions on plate. Comparison of three different grids with $\beta = 34.5°$ and $M_\infty = 2.0,\ 65 \times 65$.

ACKNOWLEDGMENTS

This project was supported by the National Natural Science Foundation of China under Grant 19582007 and by the State Key Laboratory of Scientific/Engineering Computing.

REFERENCES

1. MacCormack RW. Numerical solution of the interaction of a shock wave with a laminar boundary layer. In *Lecture Notes in Physics*, vol. 8, Holt M (ed.). Springer: Berlin, 1971; 153–163.
2. Liou M-S. A Newton/upwind method and numerical study of shock wave/boundary-layer interactions. *International Journal for Numerical Methods in Fluids* 1989; **9**: 747–761.
3. Jiang G-S, Shu C-W. Efficient implementation of weighted ENO schemes. *Journal of Computational Physics* 1996; **126**: 1202–1228.
4. Wang Z, Richards BE. High resolution schemes for steady flow computation. *Journal of Computational Physics* 1991; **97**: 53–72.
5. Sweby PK. High resolution schemes using flux limiters for hyperbolic conservation laws. *SIAM Journal of Numerical Analysis* 1984; **21**: 995–1011.
6. Chakravathy SR, Osher S. Numerical experiments with the Osher upwind scheme for the Euler equations. *AIAA Journal* 1983; **21**: 1241–1248.

